

Channel Consistency Prior and Self-Reconstruction Strategy Based Unsupervised Image Deraining

Guanglu Dong¹ Tianheng Zheng¹ Yuanzhouhan Cao² Linbo Qing¹ Chao Ren^{1*}

¹Sichuan University, Chengdu, China ²Beijing Jiaotong University, Beijing, China

{dongguanglu, zhengtianheng}@stu.scu.edu.cn, yzhcao@bjtu.edu.cn

{qing_lb, chaoren}@scu.edu.cn

Abstract

Recently, deep image deraining models based on paired datasets have made a series of remarkable progress. However, they cannot be well applied in real-world applications due to the difficulty of obtaining real paired datasets and the poor generalization performance. In this paper, we propose a novel Channel Consistency Prior and Self-Reconstruction Strategy Based Unsupervised Image Deraining framework, **CSUD**, to tackle the aforementioned challenges. During training with unpaired data, CSUD is capable of generating high-quality pseudo clean and rainy image pairs which are used to enhance the performance of deraining network. Specifically, to preserve more image background details while transferring rain streaks from rainy images to the unpaired clean images, we propose a novel Channel Consistency Loss (CCLoss) by introducing the Channel Consistency Prior (CCP) of rain streaks into training process, thereby ensuring that the generated pseudo rainy images closely resemble the real ones. Furthermore, we propose a novel Self-Reconstruction (SR) strategy to alleviate the redundant information transfer problem of the generator, further improving the deraining performance and the generalization capability of our method. Extensive experiments on multiple synthetic and real-world datasets demonstrate that the deraining performance of CSUD surpasses other state-of-the-art unsupervised methods and CSUD exhibits superior generalization capability. Code is available at <https://github.com/GuangluDong0728/CSUD>.

1. Introduction

Image deraining is an important task in low-level computer vision [7, 10, 25, 29, 31, 49]. It aims to reconstruct a clean image from its rainy version, which has a profound impact on subsequent high-level tasks such as object detection, recognition, and semantic segmentation

*Corresponding author

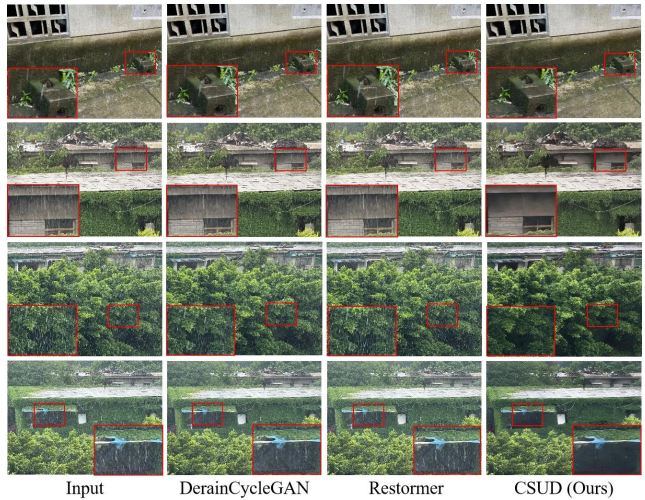


Figure 1. Deraining results on the real rainy images captured by ourselves in real-world scenarios. Compared with the supervised method Restormer [49] and the unsupervised method DerainCycleGAN [40], **our CSUD exhibits extremely strong generalization capability in the real world and achieves the best visual results.**

[24, 26, 33, 41]. To mitigate the negative impact of rain, numerous deep learning based supervised image deraining methods [7, 8, 11, 13, 19, 21, 32, 36, 47, 52] have been proposed and they achieve remarkable progress on synthetic datasets. However, the performance of these methods is largely constrained by the difficulty of capturing a large number of high-quality paired datasets when applied to real-world scenarios. Additionally, attempting to directly apply supervised models trained on synthetic datasets to real-world scenarios is also difficult because of the huge domain gap between synthetic and real-world rain [45] and the overfitting issue of supervised methods [9].

Compared to supervised methods, unsupervised deep learning methods [3, 14, 40, 42, 46] for image deraining tasks generally achieve end-to-end image deraining without paired clean-rainy images during training. This allows unsupervised methods to effectively handle complex real-world

scenarios, especially when data collection costs are high. However, due to the high difficulty and challenges of unsupervised deraining methods in training process and the lack of prior knowledge [40], there is still very little relevant research in this field. Additionally, the deraining performance of existing unsupervised methods always lags far behind that of supervised methods, and they face the same generalization issues as supervised methods.

As shown in Fig. 1, even the SOTA supervised and unsupervised deraining models [40, 49] encounter substantial generalization issues and struggle to achieve satisfactory results when dealing with rainy images captured in real world, and sometimes they even fail to remove any rain streaks due to the more complex rain distributions in real world. Based on the above analysis, how to design an effective unsupervised deraining framework to avoid the need for real paired data and how to improve the generalization performance of deraining methods have become key research issues.

In this paper, we propose a novel channel consistency prior and self-reconstruction strategy based unsupervised image deraining framework which only needs unpaired data to train the network and can be easily generalized to real-world scenarios. We first conduct detailed analysis of the channel consistency prior (CCP) of rain streaks, and then propose a novel channel consistency loss to constrain the generator to synthesize high-quality pseudo rainy images. In addition, we utilize the proposed self-reconstruction (SR) strategy to further improve the performance of the generator and enhance the generalization capability of the derainer. As shown in Figure 1, our CSUD achieves the most promising performance on the real-world captured images compared to both supervised and unsupervised deraining methods. The main contributions of this work are summarized below:

- We propose a novel channel consistency prior and self-reconstruction strategy based unsupervised image deraining framework which is able to generate high-quality pseudo paired data for training. This framework can effectively address the issues of insufficient paired data in real world and significantly improve the generalization capability of the network.
- We propose a novel channel consistency loss (CCLoss) according to the channel consistency prior (CCP) of rain streaks to enhance the performance of the generator, preserving more background details while generating pseudo rainy images. To the best of our knowledge, we are the first to incorporate CCP into the training process of unsupervised deraining framework.
- We propose a self-reconstruction (SR) strategy to solve the redundant information transfer problem of the generator. SR strategy can facilitate the accuracy of rain streaks transfer in the generator and enhance the deraining performance and the generalization capability of the derainer without altering the existing network structure.

- Extensive experiments on numerous benchmark datasets demonstrate that our proposed unsupervised framework can effectively tackle the deraining tasks on both synthetic and real-world rainy images with extremely superior generalization capability in real-world scenarios.

2. Related Works

2.1. Deep Learning Based Single Image Deraining

Supervised Single Image Deraining. Recently, with the development of deep learning, numerous excellent single image deraining [4, 5, 7, 8, 13, 21, 36, 47, 52] models have emerged. Fu et al. [7] first employ the CNN-based DerainNet to extract and remove the rain layer. Lin et al. [21] propose a generative network equipped with the pixel-wise status estimation and information decoupling for deraining. Lin et al. [23] propose a unified network for low-light-rainy image restoration to jointly handle low-light enhancement and deraining tasks. In addition to the aforementioned works specifically targeting deraining, some networks designed for image restoration [1, 16, 27, 29, 35, 38, 48, 49] have also shown excellent performance in deraining tasks. However, the above fully supervised methods require a large number of high-quality paired training samples, which is almost impossible in real-world scenarios. Simultaneously, due to the overfitting issue, their generalization capability is limited.

Unsupervised Single Image Deraining. To address the lack of paired datasets in the real world, some outstanding unsupervised deraining methods [3, 14, 40, 42, 46] have been proposed. Wei et al. [40] propose an unsupervised method for rain removal and generation by utilizing the popular CycleGAN [53] framework. Then, through introducing a dual contrastive learning manner to the CycleGAN framework, Chen et al. [3] develop an unpaired adversarial framework which effectively explores mutual properties of the unpaired rainy-clean samples. Ye et al. [46] introduce a novel non-local contrastive learning based unsupervised image deraining method to better distinguish rain streaks from clean images. However, the deraining performance of these unsupervised methods is far inferior to that of supervised methods, especially on real-world scenarios. Compared with previous methods, our proposed CSUD can greatly enhance the unsupervised deraining performance and achieve competitive results compared with some supervised methods.

2.2. Generalization Problem in Image Deraining

Deep image deraining models often fail to obtain satisfactory performance or even cannot remove any rain streaks when they are applied to real-world scenarios. Generalization problem of deraining models is an urgent issue to be solved. Gu et al. [9] conduct thorough analysis of the generalization problem in image deraining and propose to achieve better generalization by simplifying the complexity of train-

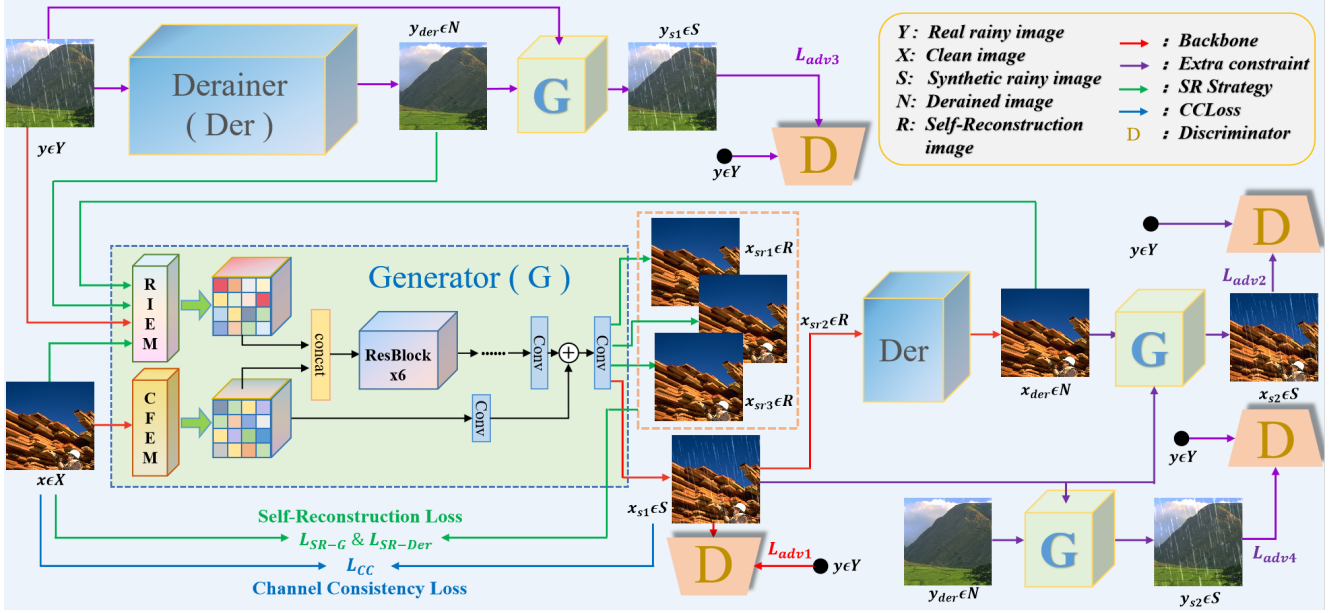


Figure 2. Framework of the proposed CSUD. The red arrows represent the baseline, purple arrows represent the 3 extra constraints, green arrows represent the self-reconstruction (SR) strategy, and blue arrows represent the CCLoss. The 4 input arrows of RIEM represent 4 separate runs of the generator, each time guided by a different image. Both RIEM and CFEM receive only 1 input image at a time.

ing images. Some semi-supervised learning frameworks [39, 44] are proposed to analyze the residual difference between domains and enhance the deraining capability in real world. In addition, a series of unsupervised deraining methods [3, 40, 46] have also demonstrated a certain degree of generalization capability in real-world scenarios. However, they have not conducted detailed analysis on how to enhance the generalization capability of unsupervised methods. Inspired by [9], we propose a self-reconstruction strategy to make both generator and derainer pay more attention to the reconstruction of image background, which significantly improves the generalization performance of our method.

3. Methodology

3.1. Overall Framework of Proposed Method

To address the issue of insufficient paired data and the generalization problem in deraining applications, we propose a novel channel consistency prior and self-reconstruction strategy based unsupervised image deraining framework, CSUD. As illustrated in Fig. 2, our CSUD consists of a derainer Der , a rainy image generator G , and a Patch-GAN [12] discriminator D . For G , it consists of a clean feature extraction module (CFEM), a rain information extraction module (RIEM) and 6 residual blocks. **Detailed network structures are detailed in the Appendix.**

In generator G , we effectively utilize unpaired clean and rainy images to synthesize pseudo rainy images. As shown by the red arrows in Fig. 2, we design a GAN-based baseline

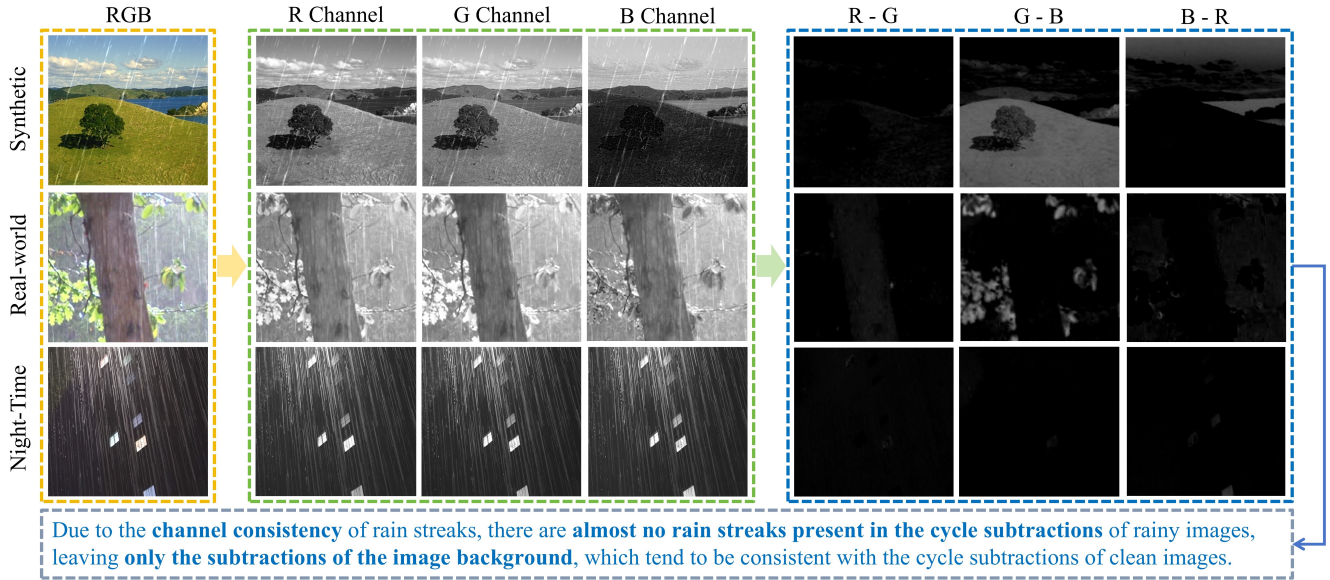
that transitions from “ $x \in X \rightarrow x_{s1} \in S \rightarrow x_{der} \in N$ ”, where X , S and N denote clean images, synthetic rainy images and derained images respectively. G transforms clean image x to synthetic rainy image x_{s1} according to the guide of real rainy image y . In order to better extract rain information and transfer it to the clean images, y and x are initially processed by the RIEM and the CFEM respectively to obtain rainy features and clean features which are concatenated for subsequent process. For the real rainy image y and the synthesized rainy image x_{s1} , the corresponding derained clean images y_{der} and x_{der} are obtained through Der .

The discriminator D is trained to distinguish between synthetic rainy images $x_{s1} \in S$ and real rainy images $y \in Y$, and the adversarial loss L_{adv1} of the baseline is constrained between them. Furthermore, motivated by existing methods [22, 53], as indicated by the purple arrows in Fig. 2, we add another three processes, $G(Der(x_{s1}), x_{s1}) \rightarrow x_{s2}$, $G(Der(y), y) \rightarrow y_{s1}$, and $G(Der(y), x_{s1}) \rightarrow y_{s2}$, to the framework to enhance training stability. Then, additional three adversarial losses are introduced to CSUD:

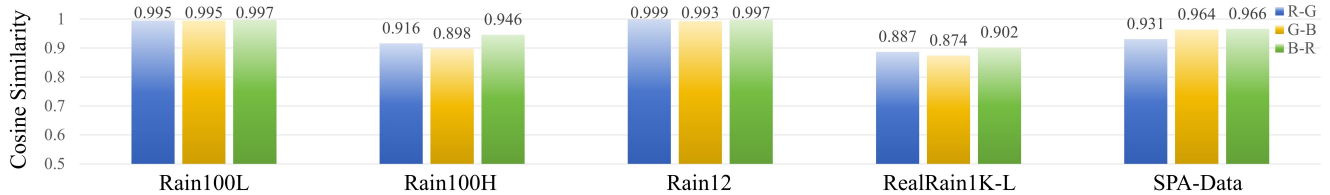
$$L_{GAN} = L_{adv1} + L_{adv2} + L_{adv3} + L_{adv4}. \quad (1)$$

3.2. Channel Consistency Loss for Generator

Channel Consistency Prior (CCP) of Rain Streaks. In RGB rainy images, most rain streaks tend to be consistent across the R, G, and B channels, meaning the pixel values of most rain streaks in the three channels are highly similar. As shown in the second, third, and fourth columns of Fig. 3 (a), we separate both synthetic and real-world rainy images



(a) Visualization of channel consistency prior in synthetic, real-world, and nighttime real-world rainy images



(b) Cosine similarities of cycle subtractions among R, G, and B channels between clean and rainy images

Figure 3. (a) Visualization of channel consistency prior in synthetic and real-world rainy images. The first column presents the rainy RGB images; the second, third and fourth columns present their R, G, B channels, respectively; the fifth, sixth, and seventh columns present the cycle subtractions of R, G, and B channels, respectively. (b) Cosine similarities of the cycle subtractions of R, G, and B channels between clean and rainy images in the 5 synthetic and real-world datasets. **More visualizations and analysis are presented in the Appendix.**

into R, G, and B channels and visualized them. It can be seen clearly that while there are significant differences in the background parts among the three channels, the rain streaks tend to be consistent. We propose to term this phenomenon as "Channel Consistency Prior (CCP)" of rainy streaks.

Theoretically, according to CCP, the cycle subtractions $((r)_R - (r)_G)$, $((r)_G - (r)_B)$, $((r)_B - (r)_R)$ of R, G, and B channels in rainy images will almost contain no rain streaks and should be close to $((n)_R - (n)_G)$, $((n)_G - (n)_B)$, $((n)_B - (n)_R)$ in clean images, where r and n represent the rainy and clean image, $(\cdot)_R$, $(\cdot)_G$, and $(\cdot)_B$ denote R, G, and B channels respectively. In the fifth, sixth, and seventh columns of Fig. 3 (a), it can be observed that the cycle subtractions of R, G, and B channels nearly don't contain any rain streaks, qualitatively confirming the correctness of CCP. Furthermore, as shown in Fig. 3 (b), we quantitatively present the cosine similarities of the cycle subtractions of R, G, and B channels between clean and rainy images in both synthetic and real-world benchmark datasets [18, 20, 36, 43]. It is evident that the cosine similarities are exceptionally high, which can further demonstrate our hypothesis.

Channel Consistency Loss. Based on the above analysis of CCP, the cycle subtractions of R, G, and B channels between input clean image and output pseudo rainy image of the generator G should tend to be consistent. To this end, we propose a novel Channel Consistency Loss (CCLoss) to preserve more color and texture details of the background while generating pseudo rainy images:

$$L_{CC} = \|((x_{s1})_R - (x_{s1})_G), (x_R - x_G)\|_1 + \|((x_{s1})_G - (x_{s1})_B), (x_G - x_B)\|_1 + \|((x_{s1})_B - (x_{s1})_R), (x_B - x_R)\|_1, \quad (2)$$

where $(x_{s1})_R$, $(x_{s1})_G$, $(x_{s1})_B$, x_R , x_G , x_B denotes R, G, B color channels of x_{s1} and x , $\|\cdot\|_1$ represents the L_1 norm and L_{CC} represents the proposed CCLoss, respectively. By introducing CCP into our unsupervised deraining framework, G will generate more accurate synthesized rainy images, which will further improve the performance of the derainer.

3.3. Self-Reconstruction Strategy

Redundant Information Transfer Problem of the Generator. Although adversarial losses can effectively constrain the

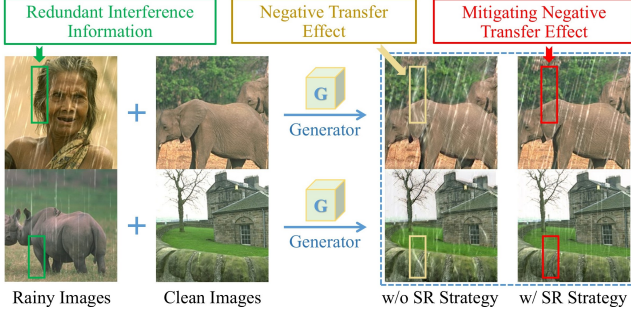


Figure 4. Visualization of redundant information transfer problem.

training process of generator G , the data synthesis process of G is highly susceptible to interference from the redundant information in rainy images, especially those edge textures that are very similar to rain streaks. As shown in Fig. 4, the edge textures of some background objects in rainy images, such as the outline of the woman’s hair, the leg of rhino, etc., are mistakenly transferred to the clean images by G . As a result, G will generate inaccurate pseudo rainy images, interfering with the learning process of Der .

Self-Reconstruction Strategy. To solve the redundant information transfer problem, we propose a novel Self-Reconstruction (SR) strategy, which enables G to extract more accurate rain streak information and synthesizes more realistic pseudo rainy images. The core idea of SR strategy is to encourage G to better distinguish rain streaks from background in the rainy images, ensuring that only rain streak information is extracted for subsequent generation of pseudo rainy images, while redundant information of background is disregarded. As shown by the green arrows in Fig. 2, when the input clean image x itself, the derained image y_{der} are input with clean image x into G , G learns to reconstruct the input clean image x itself without any additional redundant information from x and y_{der} , which means that the self-reconstructed images x_{s1} and x_{s2} should be close to x . Thus, we can utilize the following self-reconstruction loss (SRLoss) as additional training constraint of G :

$$L_{SR-G} = \|G(x, x), x\|_1 + \|G(x, y_{der}), x\|_1, \quad (3)$$

where L_{SR-G} represents the SRLoss for G . SR strategy allows G to pay more attention to reconstructing the background of clean images while learning the transfer of rain streaks, significantly improving the accuracy of generating pseudo rainy images. Under the constraint of L_{SR-G} , G will obtain the ability to generate clean images themselves guided by images without rain streaks. Therefore, the cleaner the derained images y_{der} and x_{der} restored by Der are, the closer the self-reconstructed images x_{s2} and x_{s3} are to the original clean ones x . Then, the following SRLoss can be utilized to further improve the performance of Der :

$$L_{SR-Der} = \|G(x, x_{der}), x\|_1 + \|G(x, y_{der}), x\|_1, \quad (4)$$

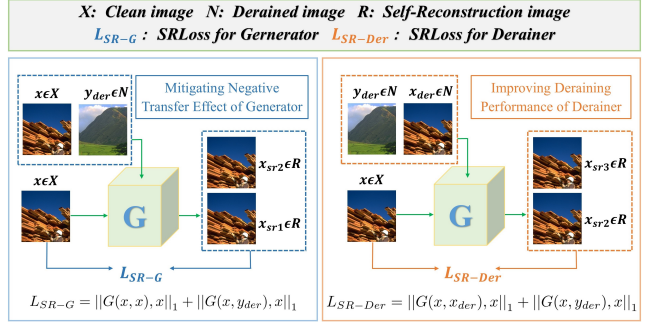


Figure 5. The implementation principles of SR strategy.

where L_{SR-Der} represents the SRLoss for Der . Under the constraint of L_{SR-Der} , Der will also focus more on reconstructing the background content while learning to derain, which greatly enhances the generalization capability of Der .

As shown in the third and fourth columns of Figure 4, SR strategy effectively alleviates the redundant information transfer problem. Through SR strategy, G can achieve robust rain streak transfer with more background detail fidelity, greatly enhancing the deraining performance of Der .

3.4. Loss Function

Due to the high difficulty and instability of training a GAN-based unsupervised framework, in addition to adopting the L1 loss for Der , we also incorporate SSIM loss and perceptual loss[15] to enhance the performance of Der :

$$L_{Der} = \|x, x_{der}\|_1 + \lambda_1 L_{SSIM}(x, x_{der}) + \lambda_2 \|\phi_i(x), \phi_i(x_{der})\|_1 + \lambda_3 L_{SR-Der}, \quad (5)$$

where $\|\cdot\|_1$ represents the L_1 norm, and $L_{SSIM}(\cdot)$ represents the SSIM loss, $\phi_i(\cdot)$ is the layers of pre-trained VGG-19 [34], $\lambda_1, \lambda_2, \lambda_3$ represent the hyperparameters for SSIM loss, perceptual loss and SRLoss for derainer respectively.

Finally, we obtain the total loss to train our framework:

$$L_{total} = \min_D \max_G L_{GAN} + L_{Der} + \alpha_1 L_{CC} + \alpha_2 L_{SR-G}, \quad (6)$$

where α_1, α_2 represent the hyperparameters for CCLoss and SRLoss for generator respectively.

4. Experiments

To demonstrate the effectiveness of our CSUD, following [18, 40], we conduct experiments from the following two aspects: (1) **unsupervised deraining performance**, (2) **generalization performance**. In experiment (1), we train independent models for different datasets respectively, including both synthetic and real-world datasets. In experiment (2), we only train our model on the synthetic dataset Rain100L [43], and then test on various real-world and nighttime datasets.

Table 1. Quantitative deraining performance comparisons of different methods. Red and blue colors indicate the 1st and 2nd ranks among the unsupervised methods, respectively. **S and U indicate supervised method and unsupervised method, respectively.**

Datasets	Rain100L [43]	Rain100H [43]	Rain12 [20]	Rain800 [17]	RealRain1K-L [18]	RealRain1K-H [18]
Metrics	PSNR	SSIM	PSNR	SSIM	PSNR	SSIM
DerainNet [7] (S)	27.03	0.884	14.92	0.592	/	/
DDN [8] (S)	32.38	0.926	24.64	0.849	34.04	0.933
SPA-Net [36] (S)	31.95	0.919	26.07	0.857	/	/
MPRNet [48] (S)	34.95	0.959	28.53	0.872	36.84	0.964
NAFNet [2] (S)	37.00	0.978	29.66	0.900	34.81	0.943
Restormer [49] (S)	37.57	0.974	29.46	0.889	/	/
PromptIR [29] (S)	38.34	0.983	28.69	0.877	35.09	0.945
NeRD-Rain-S [5] (S)	42.00	0.990	32.86	0.932	35.39	0.942
CycleGAN [53] (U)	24.61	0.834	20.59	0.704	21.56	0.845
DerainCycleGAN [40] (U)	31.49	0.936	21.13	0.710	33.52	0.940
NLCL [46] (U)	20.50	0.719	22.31	0.728	22.68	0.735
DCD-GAN [3] (U)	31.82	0.941	22.47	0.753	31.56	0.924
CSUD (Ours)	33.28	0.954	24.42	0.808	34.56	0.951

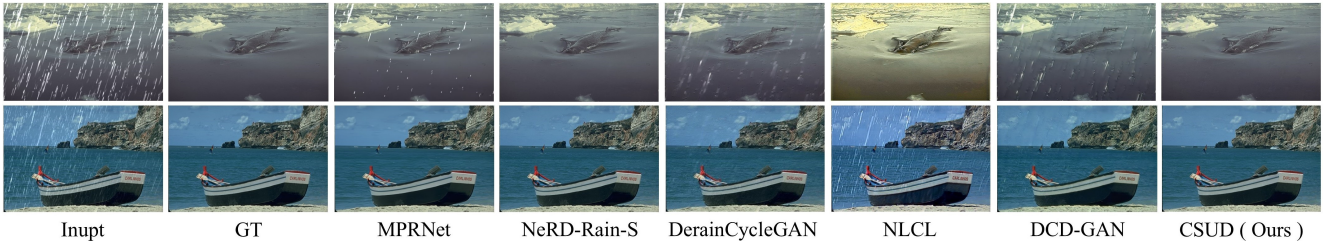


Figure 6. Qualitative deraining performance comparisons on Rain100L [43] and Rain12 [20] datasets. Our CSUD achieves competitive visual results comparable to the SOTA supervised method NeRD-Rain-S [5].

Datasets and Metrics. We utilize 10 challenging benchmark datasets in our study, including synthetic datasets: Rain100L [43], Rain100H [43], Rain12 [20], Rain800 [17], real-world datasets: RealRain1K-L [18], RealRain1K-H [18], SPA-data [36], RainDS [30], Internet-Data [39], and a nighttime dataset which is based on GTAV-NightRain dataset [50] and enlarged the rain density by [51], we name this nighttime dataset as Night-Rain in the following experiments. As for RainDS, we only use the real rain streaks subset for testing. Following existing methods [3, 40, 49], we use PSNR and SSIM [37] to evaluate different methods.

Implementation Details. As for derainer, we employ the CNN-based simple image restoration baseline NAFNet [2]. Our framework is implemented by PyTorch [28] with a GeForce RTX 3090 GPU. We adopt the Adam optimizer [6] to train our network for 200 epochs with the initial learning rate of $1e^{-4}$, followed by another 100 epochs with a learning rate of $1e^{-5}$. All training images are randomly cropped to 256×256 patches in an unpaired manner. The hyperparameters λ_1 , λ_2 , and λ_3 in Eq. 5 are set to 1, 0.2 and 0.5, while α_1 and α_2 in Eq. 6 are set to 10 and 5, respectively.

4.1. Unsupervised Deraining Results

We compare our method with unsupervised methods from the most recent years, including [3, 40, 46, 53]. Noting that the related methods for comparison are limited, since only a few

unsupervised deraining models have been proposed in the field. We also list some SOTA supervised methods, including [2, 5, 7, 8, 29, 36, 48, 49]. Tab. 1 presents the quantitative deraining results of different methods. It is evident that our CSUD significantly outperforms other unsupervised methods on most datasets. Compared to DCD-GAN[3], our CSUD respectively achieves 1.46dB, 3.00dB, and 2.22dB improvement in PSNR on Rain100L, Rain12 and RealRain1K-L datasets. Additionally, our CSUD even achieves competitive results comparable to several supervised methods. As shown in Fig. 6, compared to other unsupervised methods, our CSUD achieves better deraining results while preserving more color and texture details of image background.

4.2. Generalization Results

To validate the generalization capability of CSUD, we compare the results on 5 real-world datasets[18, 30, 36, 39] and a nighttime dataset [51] with SOTA supervised and unsupervised methods, including [2, 3, 5, 7, 29, 40, 46, 48, 49]. Noting that there are no ground truth images in the Internet-Data [39] dataset, thereby only visual results are presented. All methods are trained on synthetic datasets and tested on the unseen real-world and nighttime datasets. A prevailing perspective is that supervised methods usually outperform unsupervised methods. But as shown in Tab. 2, our CSUD almost comprehensively surpasses supervised models on

Table 2. Quantitative generalization performance comparisons of different deraining methods. Red and blue colors indicate the 1st and 2nd ranks among the unsupervised methods. **S, U indicate supervised and unsupervised methods, respectively.**

Datasets	RealRain1K-L [18]		RealRain1K-H [18]		SPA-data [36]		RainDS [30]		Night-Rain [51]	
Metrics	PSNR	SSIM	PSNR	SSIM	PSNR	SSIM	PSNR	SSIM	PSNR	SSIM
DerainNet [7] (S)	25.40	0.847	21.91	0.742	30.78	0.912	21.35	0.591	/	/
MPRNet [48] (S)	26.75	0.899	23.58	0.840	33.00	0.942	23.24	0.656	26.13	0.817
NAFNet [2] (S)	28.11	0.915	24.36	0.848	33.46	0.941	22.48	0.625	26.15	0.816
Restormer [49] (S)	26.29	0.883	23.13	0.851	32.62	0.936	22.96	0.648	25.85	0.808
PromptIR [29] (S)	28.14	0.915	24.28	0.851	33.50	0.940	22.48	0.625	26.37	0.815
NeRD-Rain-S [5] (S)	27.64	0.904	23.96	0.831	33.03	0.933	22.37	0.622	26.38	0.810
DerainCycleGAN [40] (U)	28.25	0.899	24.20	0.821	33.53	0.937	18.75	0.460	25.85	0.802
NLCL [46] (U)	20.18	0.674	19.81	0.629	18.76	0.727	17.00	0.477	22.01	0.475
DCD-GAN [3] (U)	27.49	0.912	23.86	0.845	31.55	0.930	22.13	0.610	25.54	0.798
CSUD (Ours)	29.21	0.928	25.45	0.878	33.57	0.939	22.54	0.613	25.94	0.805

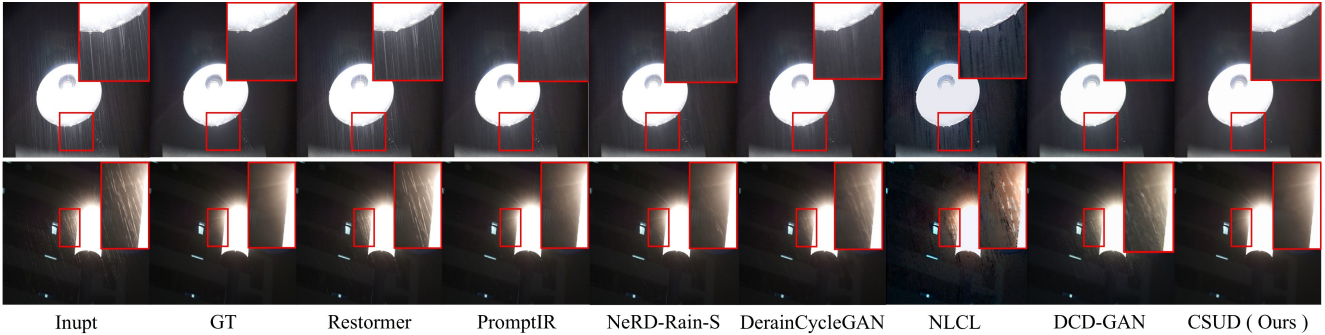


Figure 7. Qualitative generalization results on RealRain1K-L [18] and RealRain1K-H [18] real-world datasets. Our CSUD achieves best visual results among both SOTA supervised and unsupervised methods in real-world scenes.

Table 3. Effect of CCLoss and SR strategy on CSUD.

CC	SR	Rain100L[43]		Rain12[20]		RealRain1K-L[18]	
		PSNR	SSIM	PSNR	SSIM	PSNR	SSIM
✗	✗	30.66	0.925	31.60	0.931	30.42	0.932
✓	✗	31.24	0.934	32.62	0.948	31.14	0.943
✗	✓	32.69	0.949	33.43	0.939	31.86	0.950
✓	✓	33.28	0.954	34.56	0.951	32.71	0.959

the first 4 real-world datasets, while remaining competitive on the nighttime dataset. This strongly demonstrates the excellent generalization ability of our method.

As shown in Fig. 7 and Fig. 8, the performance of some most advanced supervised methods like Restormer [49] and NeRD-Rain-S [5] is extremely poor when directly applied to real-world scenarios. In contrast, our CSUD achieves better visual results in real world. It is worth mentioning again that, as shown in Fig. 1 in Sec. 1, **our method also shows extremely superior deraining performance on the rainy images captured by ourselves in real scenarios**, which further demonstrates our excellent generalization capability.

4.3. Ablation Studies

Effect of CCLoss and SR Strategy on Deraining Performance. To verify the effectiveness of CCLoss and SR strategy, we conduct ablation experiments on Rain100L [43],

Rain12 [20] and RealRain1K-L [18] datasets. As shown in Table 3, compared to the baseline, the effect on PSNR is improved by 1.38dB, 1.02dB, and 0.72dB among the above three datasets with CCLoss, respectively. And the effect is improved by 1.38dB, 1.83dB, and 1.44dB with SR strategy, respectively. Furthermore, when both CCLoss and SR strategy are introduced into the baseline, the PSNR on the three datasets is increased by 2.62dB, 2.96dB, and 2.29dB respectively. The above ablation results strongly verify the superiority and importance of CCLoss and SR strategy.

Effect of CSUD framework on Generalization Performance. To validate the effectiveness of our CSUD in improving generalization performance and the universality and robustness of our method, we also conduct experiments incorporating CSUD framework on another 2 different baselines: NeRD-Rain-S [5] and Restormer [49]. Fig. 9 shows the PSNR improvements of different CSUD based models compared to their supervised version. Notably, we train all the above models on Rain100L and test them on the 3 real-world datasets. This strongly demonstrates the effectiveness of CSUD in improving generalization performance.

Effect of Different Training Datasets on Generalization Performance. To further validate the generalization performance of CSUD, we employ 4 different CSUD models which are respectively trained on 4 synthetic and real-

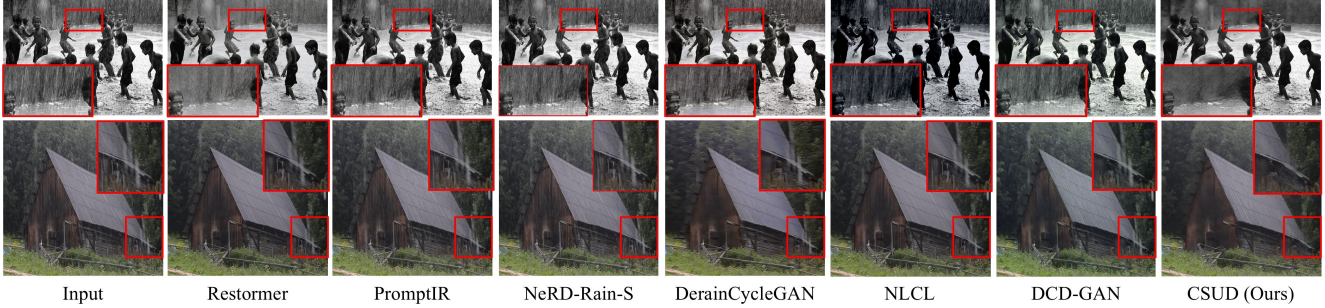


Figure 8. Qualitative generalization results on Internet-Data [39] real-world dataset.

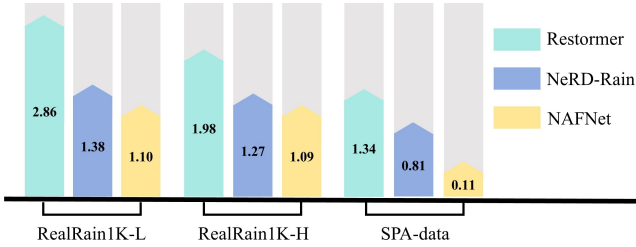


Figure 9. PSNR improvement of different baselines with CSUD. We test the models’ generalization performance on 3 real-world datasets out of domain compared with their supervised version.

Table 4. Effect of different training datasets on generalization performance. We test 4 different CSUD models which are trained on 4 different datasets on 3 real-world datasets out of domain.

Train datasets	SPA-data [36]		Night-Rain [51]		RainDS [30]	
	PSNR	SSIM	PSNR	SSIM	PSNR	SSIM
Rain100L [43]	33.57	0.939	25.94	0.805	22.54	0.613
Rain100H [43]	29.61	0.889	24.53	0.702	21.85	0.600
RealRain1K-L [18]	32.95	0.937	28.14	0.835	22.90	0.630
RealRain1K-H [18]	29.25	0.897	26.31	0.787	22.30	0.564

world datasets with different rain distributions, and test them on 3 real-world datasets. As shown in Tab. 4, in most cases, CSUD can achieve strong generalization performance, demonstrating the robustness of our approach. Due to the significant differences between rain streaks in Rain100H and real world, its generalization capability is the worst. Additionally, the generalization performance when training on Rain100L is comparable to that when training on real-world datasets, demonstrating our strong generalization ability.

Effect of the Weight Coefficients of Each Loss Function. We conduct extensive ablation experiments on the weight coefficients of perceptual loss in Eq. (5), L_{CC} and L_{SR-G} in Eq. (6). The results are shown in Tab. 5. Since L_{SR-Der} and L_{SR-G} are highly correlated, to ensure that the losses are on the same scale, the coefficient for L_{SR-Der} is set to 0.1 times that of L_{SR-G} , and L_{SR} in Tab. 5 indicates L_{SR-G} . Based on the experimental results, aside from our selected optimal combination, the deraining and generalization performance of our method remain at a high level

under most other weight combinations, demonstrating the robustness of our CSUD framework.

More detailed explanations of our method, experimental details and analysis can be found in the Appendix.

Table 5. Ablation experiments on the weight coefficients of each loss function. All models in the table are trained on Rain100L.

L_{per} (λ_2)	L_{SR} (α_2)	L_{CC} (α_1)	Rain100L [43]		SPA-data [36]		RealRain1K-L [18]	
			PSNR	SSIM	PSNR	SSIM	PSNR	SSIM
0.2	5.0	0.1	30.69	0.932	32.13	0.929	28.21	0.915
0.2	5.0	1.0	33.15	0.951	33.50	0.938	29.75	0.928
0.2	1.0	10	32.84	0.946	33.49	0.935	29.10	0.918
0.2	10	10	32.90	0.951	33.40	0.933	29.06	0.920
0	5.0	10	32.18	0.939	32.69	0.936	28.24	0.916
1.0	5.0	10	32.72	0.947	33.05	0.930	28.70	0.918
0.2	5.0	10	33.28	0.954	33.57	0.939	29.21	0.928

5. Conclusion

In this paper, we propose a novel unsupervised framework for image deraining to address the lack of paired data and the poor generalization in real-world scenarios. We first propose a channel consistency loss by introducing the channel consistency prior into the optimization process of the generator, ensuring that more background details are preserved while generating pseudo rainy images. In addition, a self-reconstruction strategy is proposed to alleviate the redundant information transfer problem and further improve the deraining performance and the generalization capability of our method. Extensive experiments on multiple synthetic and real-world datasets verify that our method achieves excellent deraining performance with strong generalization capability across various real-world rainy scenarios.

Acknowledgement. This work was supported by the National Natural Science Foundation of China under Grant 62171304 and partly by the Natural Science Foundation of Sichuan Province under Grant 2024NSFSC1423, the TCL Science and Technology Innovation Fund under grant 25JZH008, the Young Faculty Technology Innovation Capacity Enhancement Program of Sichuan University under Grant 2024SCUQJTX025, and the Beijing Natural Science Foundation L221011.

References

- [1] Liangyu Chen, Xin Lu, Jie Zhang, Xiaojie Chu, and Chengpeng Chen. Hinet: Half instance normalization network for image restoration. In *Proceedings of the IEEE/CVF conference on computer vision and pattern recognition*, pages 182–192, 2021. **2**
- [2] Liangyu Chen, Xiaojie Chu, Xiangyu Zhang, and Jian Sun. Simple baselines for image restoration. In *European conference on computer vision*, pages 17–33. Springer, 2022. **6, 7, 3, 5**
- [3] Xiang Chen, Jinshan Pan, Kui Jiang, Yufeng Li, Yufeng Huang, Caihua Kong, Longgang Dai, and Zhentao Fan. Unpaired deep image deraining using dual contrastive learning. In *Proceedings of the IEEE/CVF conference on computer vision and pattern recognition*, pages 2017–2026, 2022. **1, 2, 3, 6, 7, 5**
- [4] Xiang Chen, Hao Li, Mingqiang Li, and Jinshan Pan. Learning a sparse transformer network for effective image deraining. In *Proceedings of the IEEE/CVF Conference on Computer Vision and Pattern Recognition*, pages 5896–5905, 2023. **2**
- [5] Xiang Chen, Jinshan Pan, and Jiangxin Dong. Bidirectional multi-scale implicit neural representations for image deraining. In *Proceedings of the IEEE/CVF Conference on Computer Vision and Pattern Recognition*, pages 25627–25636, 2024. **2, 6, 7, 1, 5**
- [6] P Kingma Diederik. Adam: A method for stochastic optimization. (*No Title*), 2014. **6, 4**
- [7] Xueyang Fu, Jiabin Huang, Xinghao Ding, Yinghao Liao, and John Paisley. Clearing the skies: A deep network architecture for single-image rain removal. *IEEE Transactions on Image Processing*, 26(6):2944–2956, 2017. **1, 2, 6, 7**
- [8] Xueyang Fu, Jiabin Huang, Delu Zeng, Yue Huang, Xinghao Ding, and John Paisley. Removing rain from single images via a deep detail network. In *Proceedings of the IEEE conference on computer vision and pattern recognition*, pages 3855–3863, 2017. **1, 2, 6**
- [9] Jinjin Gu, Xianzheng Ma, Xiangtao Kong, Yu Qiao, and Chao Dong. Networks are slacking off: Understanding generalization problem in image deraining. *Advances in Neural Information Processing Systems*, 36, 2023. **1, 2, 3**
- [10] Kaiming He, Jian Sun, and Xiaoou Tang. Single image haze removal using dark channel prior. *IEEE transactions on pattern analysis and machine intelligence*, 33(12):2341–2353, 2010. **1**
- [11] Xiaowei Hu, Chi-Wing Fu, Lei Zhu, and Pheng-Ann Heng. Depth-attentional features for single-image rain removal. In *Proceedings of the IEEE/CVF Conference on computer vision and pattern recognition*, pages 8022–8031, 2019. **1**
- [12] Phillip Isola, Jun-Yan Zhu, Tinghui Zhou, and Alexei A Efros. Image-to-image translation with conditional adversarial networks. In *Proceedings of the IEEE conference on computer vision and pattern recognition*, pages 1125–1134, 2017. **3, 4**
- [13] Kui Jiang, Zhongyuan Wang, Peng Yi, Chen Chen, Baojin Huang, Yimin Luo, Jiayi Ma, and Junjun Jiang. Multi-scale progressive fusion network for single image deraining. In *Proceedings of the IEEE/CVF conference on computer vision and pattern recognition*, pages 8346–8355, 2020. **1, 2**
- [14] Xin Jin, Zhibo Chen, Jianxin Lin, Zhikai Chen, and Wei Zhou. Unsupervised single image deraining with self-supervised constraints. In *2019 IEEE International Conference on Image Processing (ICIP)*, pages 2761–2765. IEEE, 2019. **1, 2**
- [15] Justin Johnson, Alexandre Alahi, and Li Fei-Fei. Perceptual losses for real-time style transfer and super-resolution. In *Computer Vision–ECCV 2016: 14th European Conference, Amsterdam, The Netherlands, October 11–14, 2016, Proceedings, Part II 14*, pages 694–711. Springer, 2016. **5**
- [16] Boyun Li, Xiao Liu, Peng Hu, Zhongqin Wu, Jiancheng Lv, and Xi Peng. All-in-one image restoration for unknown corruption. In *Proceedings of the IEEE/CVF conference on computer vision and pattern recognition*, pages 17452–17462, 2022. **2**
- [17] Siyuan Li, Iago Breno Araujo, Wenqi Ren, Zhangyang Wang, Eric K Tokuda, Roberto Hirata Junior, Roberto Cesar-Junior, Jiawan Zhang, Xiaojie Guo, and Xiaochun Cao. Single image deraining: A comprehensive benchmark analysis. In *Proceedings of the IEEE/CVF Conference on Computer Vision and Pattern Recognition*, pages 3838–3847, 2019. **6, 4, 5**
- [18] Wei Li, Qiming Zhang, Jing Zhang, Zhen Huang, Xinmei Tian, and Dacheng Tao. Toward real-world single image deraining: A new benchmark and beyond. *arXiv preprint arXiv:2206.05514*, 2022. **4, 5, 6, 7, 8**
- [19] Xia Li, Jianlong Wu, Zhouchen Lin, Hong Liu, and Hongbin Zha. Recurrent squeeze-and-excitation context aggregation net for single image deraining. In *Proceedings of the European conference on computer vision (ECCV)*, pages 254–269, 2018. **1**
- [20] Yu Li, Robby T Tan, Xiaojie Guo, Jiangbo Lu, and Michael S Brown. Rain streak removal using layer priors. In *Proceedings of the IEEE conference on computer vision and pattern recognition*, pages 2736–2744, 2016. **4, 6, 7, 5**
- [21] Di Lin, Xin Wang, Jia Shen, Renjie Zhang, Ruonan Liu, Miao-hui Wang, Wuyuan Xie, Qing Guo, and Ping Li. Generative status estimation and information decoupling for image rain removal. *Advances in Neural Information Processing Systems*, 35:4612–4625, 2022. **1, 2**
- [22] Xin Lin, Chao Ren, Xiao Liu, Jie Huang, and Yinjie Lei. Unsupervised image denoising in real-world scenarios via self-collaboration parallel generative adversarial branches. In *Proceedings of the IEEE/CVF International Conference on Computer Vision*, pages 12642–12652, 2023. **3**
- [23] Xin Lin, Jingtong Yue, Sixian Ding, Chao Ren, Chun-Le Guo, and Chongyi Li. Unlocking low-light-rainy image restoration by pairwise degradation feature vector guidance. *arXiv preprint arXiv:2305.03997*, 2023. **2**
- [24] Li Liu, Wanli Ouyang, Xiaogang Wang, Paul Fieguth, Jie Chen, Xinwang Liu, and Matti Pietikäinen. Deep learning for generic object detection: A survey. *International journal of computer vision*, 128:261–318, 2020. **1**
- [25] Xiao Liu, Xiangyu Liao, Xiuya Shi, Linbo Qing, and Chao Ren. Efficient information modulation network for image super-resolution. In *ECAI 2023*, pages 1544–1551. IOS Press, 2023. **1**
- [26] Xiao Liu, Xiuya Shi, Lufei Chen, Linbo Qing, and Chao Ren. Efficient parallel multi-scale detail and semantic encoding network for lightweight semantic segmentation. In *Proceedings*

- of the 31st ACM International Conference on Multimedia, pages 2544–2552, 2023. 1
- [27] Dongwon Park, Byung Hyun Lee, and Se Young Chun. All-in-one image restoration for unknown degradations using adaptive discriminative filters for specific degradations. In *2023 IEEE/CVF Conference on Computer Vision and Pattern Recognition (CVPR)*, pages 5815–5824. IEEE, 2023. 2
- [28] Adam Paszke, Sam Gross, Francisco Massa, Adam Lerer, James Bradbury, Gregory Chanan, Trevor Killeen, Zeming Lin, Natalia Gimelshein, Luca Antiga, et al. Pytorch: An imperative style, high-performance deep learning library. *Advances in neural information processing systems*, 32, 2019. 6, 4
- [29] Vaishnav Potlapalli, Syed Waqas Zamir, Salman H Khan, and Fahad Shahbaz Khan. Promptir: Prompting for all-in-one image restoration. *Advances in Neural Information Processing Systems*, 36, 2023. 1, 2, 6, 7, 5
- [30] Ruijie Quan, Xin Yu, Yuanzhi Liang, and Yi Yang. Removing raindrops and rain streaks in one go. In *Proceedings of the IEEE/CVF conference on computer vision and pattern recognition*, pages 9147–9156, 2021. 6, 7, 8, 4
- [31] Chao Ren, Yizhong Pan, and Jie Huang. Enhanced latent space blind model for real image denoising via alternative optimization. *Advances in Neural Information Processing Systems*, 35:38386–38399, 2022. 1
- [32] Dongwei Ren, Wangmeng Zuo, Qinghua Hu, Pengfei Zhu, and Deyu Meng. Progressive image deraining networks: A better and simpler baseline. In *Proceedings of the IEEE/CVF conference on computer vision and pattern recognition*, pages 3937–3946, 2019. 1
- [33] Shaoqing Ren, Kaiming He, Ross Girshick, and Jian Sun. Faster r-cnn: Towards real-time object detection with region proposal networks. *IEEE transactions on pattern analysis and machine intelligence*, 39(6):1137–1149, 2016. 1
- [34] Karen Simonyan and Andrew Zisserman. Very deep convolutional networks for large-scale image recognition. *arXiv preprint arXiv:1409.1556*, 2014. 5
- [35] Cong Wang, Jinshan Pan, Wei Wang, Jiangxin Dong, Mengzhu Wang, Yakun Ju, and Junyang Chen. Promptrestorer: A prompting image restoration method with degradation perception. *Advances in Neural Information Processing Systems*, 36:8898–8912, 2023. 2
- [36] Tianyu Wang, Xin Yang, Ke Xu, Shaozhe Chen, Qiang Zhang, and Rynson WH Lau. Spatial attentive single-image deraining with a high quality real rain dataset. In *Proceedings of the IEEE/CVF conference on computer vision and pattern recognition*, pages 12270–12279, 2019. 1, 2, 4, 6, 7, 8
- [37] Zhou Wang, Alan C Bovik, Hamid R Sheikh, and Eero P Simoncelli. Image quality assessment: from error visibility to structural similarity. *IEEE transactions on image processing*, 13(4):600–612, 2004. 6
- [38] Zhendong Wang, Xiaodong Cun, Jianmin Bao, Wengang Zhou, Jianzhuang Liu, and Houqiang Li. Uformer: A general u-shaped transformer for image restoration. In *Proceedings of the IEEE/CVF conference on computer vision and pattern recognition*, pages 17683–17693, 2022. 2
- [39] Wei Wei, Deyu Meng, Qian Zhao, Zongben Xu, and Ying Wu. Semi-supervised transfer learning for image rain removal. In *Proceedings of the IEEE/CVF conference on computer vision and pattern recognition*, pages 3877–3886, 2019. 3, 6, 8, 4, 7
- [40] Yanyan Wei, Zhao Zhang, Yang Wang, Mingliang Xu, Yi Yang, Shuicheng Yan, and Meng Wang. Deraincyclegan: Rain attentive cyclegan for single image deraining and rainmaking. *IEEE Transactions on Image Processing*, 30:4788–4801, 2021. 1, 2, 3, 5, 6, 7, 4
- [41] Zbigniew Wojna, Vittorio Ferrari, Sergio Guadarrama, Nathan Silberman, Liang-Chieh Chen, Alireza Fathi, and Jasper Uijlings. The devil is in the decoder: Classification, regression and gans. *International Journal of Computer Vision*, 127: 1694–1706, 2019. 1
- [42] Wei Xu, Xinyuan Chen, Haoming Guo, Xiaolin Huang, and Wei Liu. Unsupervised image restoration with quality-task-perception loss. *IEEE Transactions on Circuits and Systems for Video Technology*, 32(9):5736–5747, 2022. 1, 2
- [43] Wenhan Yang, Robby T Tan, Jiashi Feng, Zongming Guo, Shuicheng Yan, and Jiaying Liu. Joint rain detection and removal from a single image with contextualized deep networks. *IEEE transactions on pattern analysis and machine intelligence*, 42(6):1377–1393, 2019. 4, 5, 6, 7, 8
- [44] Rajeev Yasarla, Vishwanath A Sindagi, and Vishal M Patel. Syn2real transfer learning for image deraining using gaussian processes. In *Proceedings of the IEEE/CVF conference on computer vision and pattern recognition*, pages 2726–2736, 2020. 3
- [45] Yuntong Ye, Yi Chang, Hanyu Zhou, and Luxin Yan. Closing the loop: Joint rain generation and removal via disentangled image translation. In *Proceedings of the IEEE/CVF conference on computer vision and pattern recognition*, pages 2053–2062, 2021. 1
- [46] Yuntong Ye, Changfeng Yu, Yi Chang, Lin Zhu, Xi-Le Zhao, Luxin Yan, and Yonghong Tian. Unsupervised deraining: Where contrastive learning meets self-similarity. In *Proceedings of the IEEE/CVF conference on computer vision and pattern recognition*, pages 5821–5830, 2022. 1, 2, 3, 6, 7, 5
- [47] Qiaosi Yi, Juncheng Li, Qinyan Dai, Faming Fang, Guixu Zhang, and Tiejong Zeng. Structure-preserving deraining with residue channel prior guidance. In *Proceedings of the IEEE/CVF international conference on computer vision*, pages 4238–4247, 2021. 1, 2
- [48] Syed Waqas Zamir, Aditya Arora, Salman Khan, Munawar Hayat, Fahad Shahbaz Khan, Ming-Hsuan Yang, and Ling Shao. Multi-stage progressive image restoration. In *Proceedings of the IEEE/CVF conference on computer vision and pattern recognition*, pages 14821–14831, 2021. 2, 6, 7, 5
- [49] Syed Waqas Zamir, Aditya Arora, Salman Khan, Munawar Hayat, Fahad Shahbaz Khan, and Ming-Hsuan Yang. Restormer: Efficient transformer for high-resolution image restoration. In *Proceedings of the IEEE/CVF conference on computer vision and pattern recognition*, pages 5728–5739, 2022. 1, 2, 6, 7, 5
- [50] Fan Zhang, Shaodi You, Yu Li, and Ying Fu. Gtavn-nightrain: Photometric realistic large-scale dataset for night-time rain streak removal. *arXiv preprint arXiv:2210.04708*, 2022. 6
- [51] Fan Zhang, Shaodi You, Yu Li, and Ying Fu. Learning rain location prior for nighttime deraining. In *Proceedings of*

the IEEE/CVF International Conference on Computer Vision, pages 13148–13157, 2023. [6](#), [7](#), [8](#), [4](#)

- [52] He Zhang and Vishal M Patel. Density-aware single image de-raining using a multi-stream dense network. In *Proceedings of the IEEE conference on computer vision and pattern recognition*, pages 695–704, 2018. [1](#), [2](#)
- [53] Jun-Yan Zhu, Taesung Park, Phillip Isola, and Alexei A Efros. Unpaired image-to-image translation using cycle-consistent adversarial networks. In *Proceedings of the IEEE international conference on computer vision*, pages 2223–2232, 2017. [2](#), [3](#), [6](#)

Channel Consistency Prior and Self-Reconstruction Strategy Based Unsupervised Image Deraining

Supplementary Material

In this paper, we propose a novel Channel Consistency Prior and Self-Reconstruction Strategy based Unsupervised Image Deraining framework, **CSUD**, to address the lack of paired data and the poor generalization in real-world scenarios. Extensive experiments on multiple synthetic and real-world datasets verify that our method achieves excellent deraining performance. What’s more, as shown in Fig. 1, our CSUD achieves the most promising performance on the real-world captured images compared to both supervised and unsupervised deraining methods, which demonstrates strong generalization capability of our CSUD. This supplementary material mainly includes the following contents:

- More detailed explanations of the proposed channel consistency prior and self-reconstruction strategy;
- The specific structure of certain used networks;
- More implementation details of the experiments mentioned in the main document;
- Additional experiment results and analysis;
- Discussion and limitations of our method.

1. More Explanations of Channel Consistency Prior

In the main document, we have provided a detailed introduction to the channel consistency prior (CCP) of rain streaks: in RGB rainy images, most rain streaks tend to be consistent across the R, G, and B channels, and the cycle subtractions of R, G, and B channels in rainy images will almost contain no rain streaks and should be close to the cycle subtractions in clean images. To present the conclusions derived from CCP more clearly and intuitively, we provide a more detailed visualization of the CCP in rainy images along with the corresponding clean images in Fig. 2, including synthetic rain, real-world rain, and real-world nighttime rain. We can clearly observe that while there are significant differences in the background parts among the three channels of rainy images, the rain streaks tend to be consistent, and the cycle subtractions of R, G, and B channels in rainy images tend to be consistent with that of their corresponding clean images.

Currently, the rain in an image is typically modeled using the linear superposition model: $Y = X + R$, where Y is the rainy image, R is the rain layer, and X is the image background. Most image deraining researches [3–5, 7, 21, 40, 52] focuses on the removal of the rain layer R in images. One of the reasons why many unsupervised image deraining models perform poorly is that, while they remove rain layer, they struggle to maintain the integrity of other background information in the image. In this work, we also mainly focus on

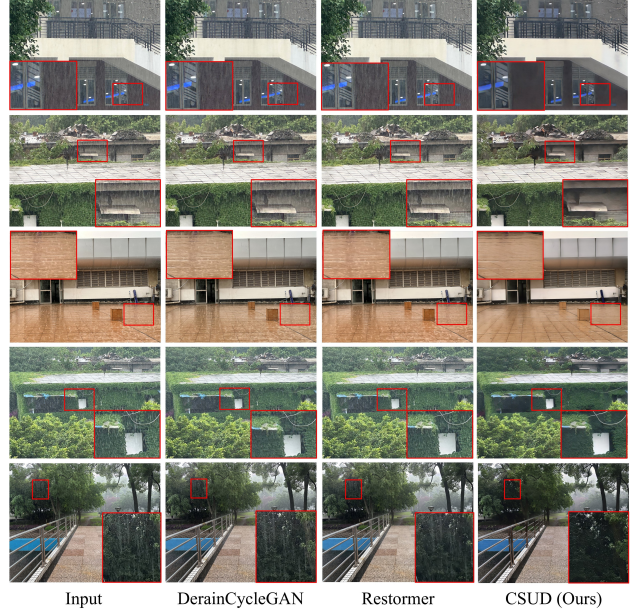


Figure 1. Deraining results on the real rainy images captured by ourselves in real-world scenarios. Compared with the supervised method Restormer [49] and the unsupervised method DerainCycleGAN [40], our CSUD exhibits extremely strong generalization capability and achieves the best visual results.

removing rain layer R from rainy images. During training, the derainer learns the mapping between pseudo-rainy images and real clean images X . If the pseudo-rainy images maintain the main background information of X , differing from clean images only by the presence of the rain streaks, the derainer will learn the optimal mapping relationship. Thus, we introduce the Channel Consistency Loss (CCLoss) to constrain the generator G to produce pseudo-rainy images that retain most of the image content consistent with the original clean images X aside from the rain streaks. Through the constrain of CCLoss, the derainer can better learn the desired mapping.

In addition, we separately analyze the special cases which include nighttime artificial light sources. As shown in Fig. 3, we provide a visualization of CCP **under the nighttime artificial light scenario**. While the rain streaks in rainy image appear yellowish due to interference from artificial light, the rain streaks in the residual image do not exhibit such yellowish tones, and most rain streaks still conform to CCP among R,G,B channels. According to the linear superposition model, rainy images can be understood as the superposition of the rain layer and the clean background.

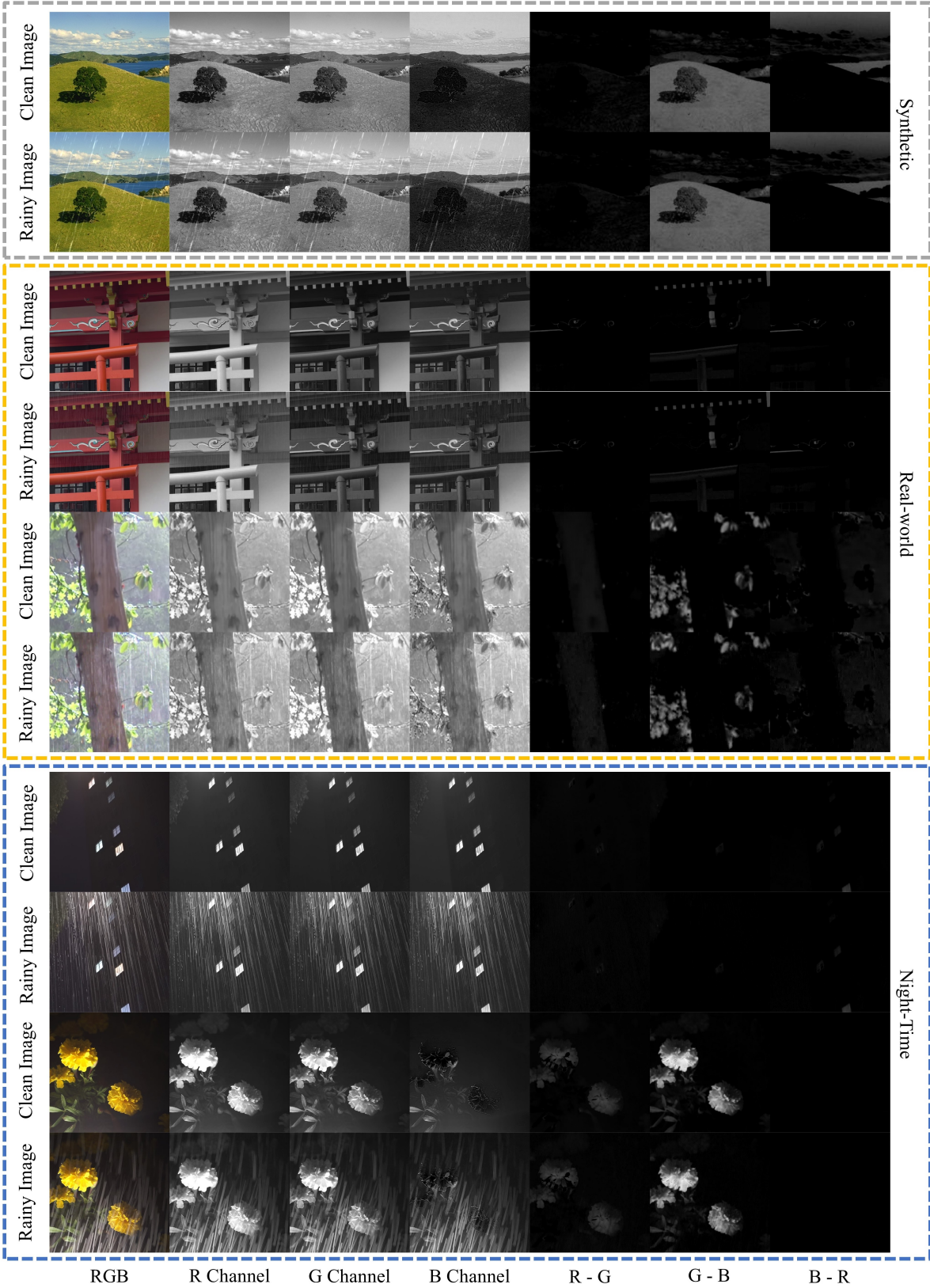


Figure 2. Visualization of channel consistency prior in rainy images. From top to bottom, the 3 sets of images are synthetic, real-world, and real-world nighttime images, respectively. The first column presents the clean and rainy RGB images; the second, third and fourth columns present their R, G, B channels, respectively; the fifth, sixth, and seventh columns present the cycle subtractions of R, G, and B channels of clean and rainy images, respectively.

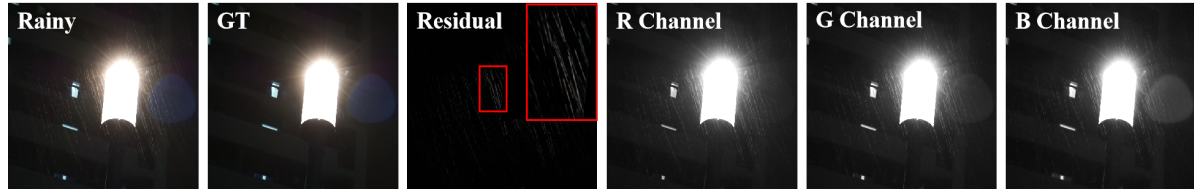


Figure 3. Visualization of channel consistency prior under the nighttime artificial light scenario.

Therefore, the yellowish hue in rain streaks is the color of the background introduced by artificial light. Furthermore, in Fig.7, Tab.1, and Tab.2 of the main text, we test our model on real-world datasets RealRain1K-L and RealRain1K-H which **include numerous nighttime artificial light sources**, and our CSUD achieves remarkable results.

Certainly, there may be some rain streaks that do not adhere to the CCP, but this does not significantly affect the network’s performance. This is because, besides CCP, the SR strategy and overall unsupervised framework with the three additional constraints based on CycleGAN [53] can also ensure the accurate and effective generation of pseudo-paired rainy images, as well as the deraining and generalization performance of CSUD. The CCLoss serves as a further auxiliary enhancement to the overall framework, aiming to transfer rain streaks while preserving more background details as much as possible, which makes our framework more robust. It is the combined effort of our unsupervised framework, CCLoss, and the SR strategy that achieves the outstanding unsupervised deraining performance of CSUD.

2. More Explanation of Self-Reconstruction Strategy

As described in main document, x_{der} restored by derainer Der is not adopted in SRLoss for generator L_{SR-G} . However, x_{der} can also be used in L_{SR-G} to constrain the training process of generator G , but we do not add it in the final implementation in order to make the SR loss for generator L_{SR-G} and SR loss for derainer L_{SR-Der} on the same scale and reduce the calculation of the training process, which has little effect on the performance of the network. Additionally, as shown in Fig. 4, we present more visualizations of the effects of SR strategy on the performance of generator G . With SR strategy, the generator effectively alleviates the redundant information transfer problem, ensuring that higher-quality pseudo rainy images are generated.

3. Detailed Network Structures.

As described in the main document, the proposed CSUD mainly consists of a derainer, a generator, and a discriminator. To balance the performance and computational complexity, we adopt the simple CNN-based image restoration baseline NAFNet [2] (the version of width32) as the default derainer.

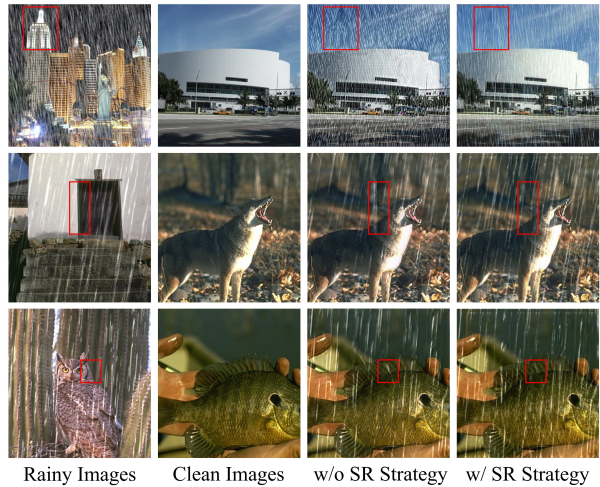


Figure 4. The effects of SR strategy on the performance of generator. The first and second columns present the input rainy and clean images of the generator, respectively; the third column presents pseudo rainy images generated by the generator without SR strategy; the fourth column presents pseudo rainy images generated by the generator with SR strategy.

Architecture of the Generator. The architecture of the generator used in our network is shown in Fig. 5, it consists of a clean feature extraction module (CFEM), a rain information extraction module (RIEM) and 6 residual blocks. The RIEM is based on a U-Net architecture, comprising a downsampling layer followed by an upsampling layer, while the CFEM simply utilize a convolutional layer. Specifically, the two convolutional layers in RIEM (denoted as “conv”) have input channels, output channels, kernel size, stride, and padding settings of [3, 64, 7, 1, 3] and [64, 64, 7, 1, 3], respectively. The downsampling layer in RIEM is a convolutional layer with input channels, output channels, kernel size, stride, and padding set to [64, 128, 4, 2, 1]. The upsampling layer in RIEM uses a ‘bilinear’ interpolation, followed by a convolutional layer with input channels, output channels, kernel size, stride, and padding set to [128, 64, 3, 1, 1]. The convolutional layer in CFEM has input channels, output channels, kernel size, stride, and padding set to [3, 64, 7, 1, 3]. Each residual block consists of two 3×3 convolution layers with ReLU activation function. The generator learns the rain characteristics of rainy images to guide the synthesis

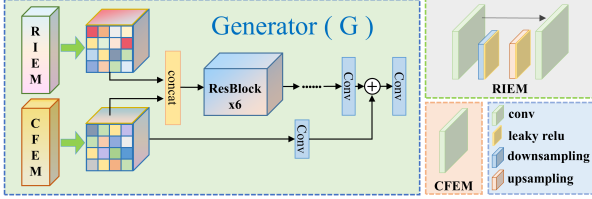


Figure 5. Detailed network structures of the generator.

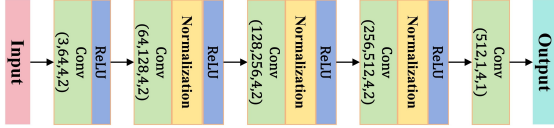


Figure 6. Detailed network structures of the discriminator.

of clean images towards rainy ones, providing ample pseudo rainy images paired with the clean ones for the derainer.

Architecture of the Discriminator. In our network, we use a Patch-GAN [12] discriminator, as shown in Fig. 6. The discriminator is starting with a 4×4 convolution layer with ReLU activation function, followed by three intermediate layers, each of which consists of instance normalization between the convolution layer and the activation function, and ending with a 4×4 convolution layer with a stride of 1.

4. More Explanation of Experiment Setting

As described in the main document, following [18, 40], we conduct experiments from two aspects: (1) unsupervised deraining performance and (2) generalization performance. In experiment (2), we only train our model on the synthetic dataset Rain100L [43], and then test on various real-world and nighttime datasets. This experimental setup is designed to better demonstrate the strong cross-domain generalization ability of our CSUD framework, specifically its deraining performance when faced with various rain streak distributions, rather than suggesting that our CSUD should be trained exclusively on synthetic datasets for optimal performance. Our CSUD can also be trained on unpaired real-world datasets and achieve better performance. In the main document, we have conducted experiments on the real-world RealRain-1k-L and RealRain-1k-H datasets according to the experiment (1) settings. Trained on unpaired real-world datasets, CSUD achieves better results on the two real-world datasets, even surpassing some classic supervised methods.

5. Experiment Details

Datasets. Detailed descriptions of the datasets employed are provided in Tab. 1. In experiment (1), we use the corresponding different training sets to train independent models for Rain100L [43], Rain100H [43], Rain800 [17], RealRain1K-L [18], and RealRain1K-H [18] test sets respectively. Notably, we utilize the model trained on Rain100L to test on

Table 1. Detailed description of the datasets utilized.

Datasets	Rain100L [43]	Rain100H [43]	Rain12 [20]	Rain800 [17]	RealRain1K-L [18]
Train	200	200	0	700	784
Test	100	100	12	100	224
Rain Type	Synthetic	Synthetic	Synthetic	Synthetic	Real-world

Datasets	RealRain1K-H [18]	SPA-data [36]	RainDS [30]	Internet-Data [39]	Night-Rain [51]
Train	784	638,492	150	0	5000
Test	224	1000	98	147	500
Rain Type	Real-world	Real-world	Real-world	Real-world	Night-Time

Rain12 [20] dataset. As for experiment (2), we only train our model on Rain100L [43], and then test on the 6 real-world and night-time test sets, including RealRain1K-L [18], RealRain1K-H [18], SPA-data [36], RainDS [30], Internet-Data [39], and Night-Rain [51]. It is worth noting that RainDS includes multiple subsets, including synthetic and real subsets, with the two subsets further divided into rain streaks, rain drops, and a mixture of rain streaks and drops. Since our method focuses on removing rain streaks and experiment (2) is to evaluate generalization performance on real-world and night-time test sets, so we only select the rain streaks subset from the real RainDS subset for testing. All other comparison models are also tested on this subset.

Implementation Details. Our framework is implemented by PyTorch [28] with a GeForce RTX 3090 GPU. For training, we adopt the Adam optimizer [6] ($\beta_1 = 0.9$, $\beta_2 = 0.999$) to train our network. We train the framework for 200 epochs with the initial learning rate of $1e^{-4}$, followed by another 100 epochs with a learning rate of $1e^{-5}$. All training images are randomly cropped to 256×256 patches in an unpaired learning manner, and the batch size is set to 2. The hyperparameters of SSIM loss (λ_1), perceptual loss (λ_2), and SRLoss for derainer (λ_3) are set to 1, 0.2 and 0.5 respectively, while CCLoss (α_1) and SRLoss for generator (α_2) are set to 10 and 5 respectively. Notably, we add perceptual loss to our framework is not to improve perceptual quality of our results, but to enhance the stability of the unsupervised training process. Because we find that only using L1 loss as the constraint of the derainer will collapse in the middle of the training process, which is caused by the difficulty and instability of the GAN manner. For fair comparison, all PSNR and SSIM scores reported in the main document are calculated on the RGB channels. The results of other methods are directly cited from the original papers or generated using the official models. For the results on datasets that the authors did not report or test, we retrain their models using the official code provided by the authors.

6. More Experiment Results

We present more experiment results on unsupervised deraining performance and generalization performance to further elucidate the effectiveness of the proposed CSUD.

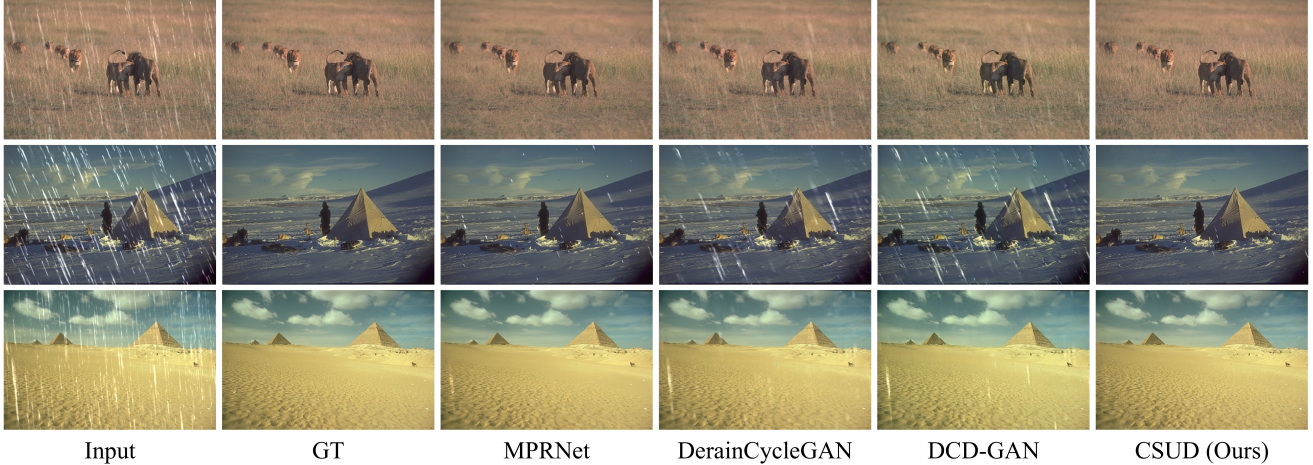


Figure 7. Qualitative deraining results on Rain100L [43] dataset.

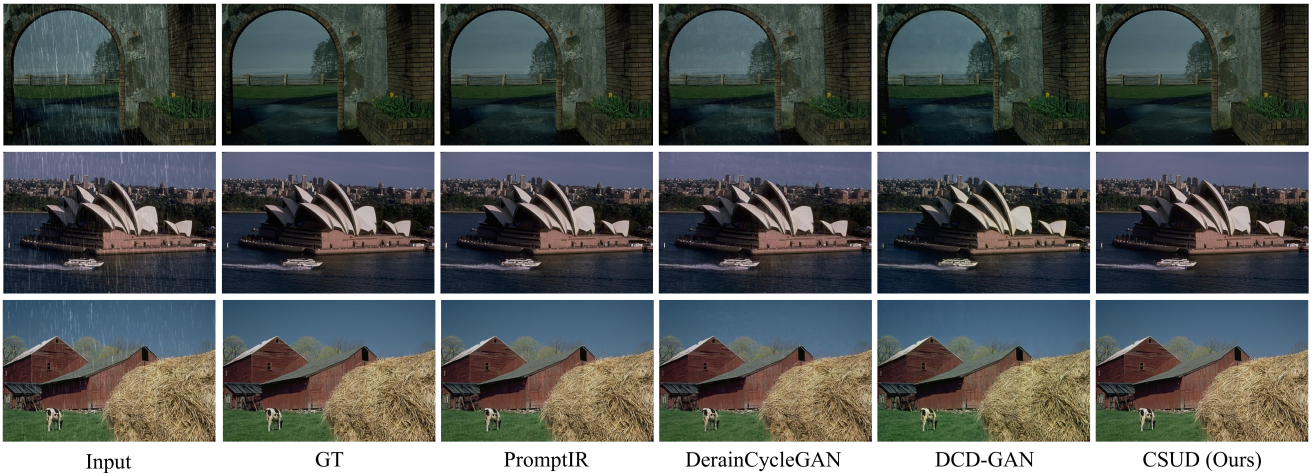


Figure 8. Qualitative deraining results on Rain12 [20] dataset.

6.1. Unsupervised Deraining Results

We provide additional visual comparisons on benchmark datasets in Fig. 7, Fig. 8, and Fig. 9. We compare our CSUD with several recent state-of-the-art unsupervised and supervised image deraining methods, including [3, 29, 40, 46, 48]. As shown in the figures, it can be seen that our CSUD achieves better results in removing rain streaks compared to other unsupervised methods and our CSUD preserves more texture details of image background. It is worth noting that there is a certain background color offset between the input and GT images of Rain800 dataset [17], however, our CSUD aims to preserve more color and texture details of image background while removing rain streaks, so our quantitative results in the main document which are are not the best.

6.2. Generalization Deraining Results

To validate the generalization capability of CSUD, we provide more additional visual comparisons with other un-

supervised and supervised deraining methods, including [3, 29, 40, 46, 49] in Fig. 12, Fig. 11, and Fig. 10. All methods are trained on synthetic datasets and tested on the unseen real-world datasets. Compared to other methods, our CSUD achieves better visual results in real-world scenarios, which demonstrates the excellent generalization capability of CSUD.

6.3. More Ablation Studies

Effect of CSUD framework on perceptual quality. To more comprehensively evaluate the performance of our CSUD in real world, we select 3 deraining baselines MPRNet [48], NeRD-Rain-S [5], and NAFNet [2], and we use additional perceptual quality metrics to test their supervised version and unsupervised version with our CSUD on 3 real-world datasets. The perceptual quality metrics includes full-reference metrics: LPIPS [?], DISTS [?] and no-reference metric: NIQE [?]. As shown in Tab. 2, our CSUD achieves

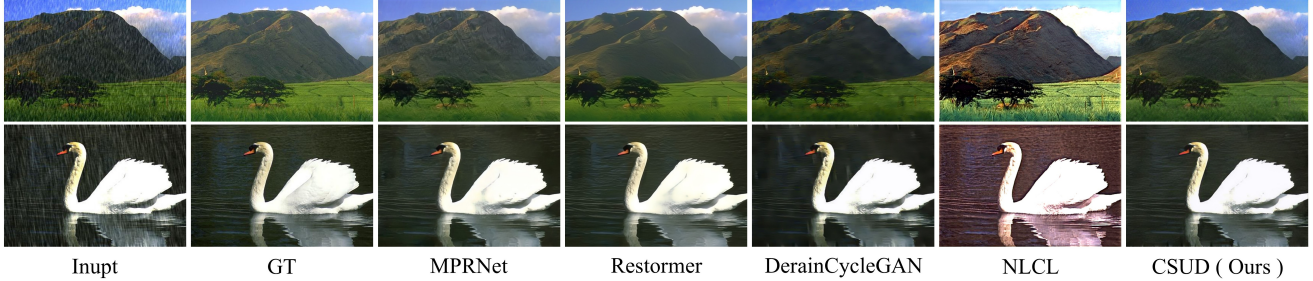


Figure 9. Qualitative deraining results on Rain800 [17] dataset.

Table 2. Quantitative perceptual quality comparisons of different deraining baselines with or without our methods.

Datasets	RealRain1K-L [18]	RealRain1K-H [18]	SPA-data [36]
Metrics	LPIPS ↓ / DISTs ↓ / NIQE ↓	LPIPS ↓ / DISTs ↓ / NIQE ↓	LPIPS ↓ / DISTs ↓ / NIQE ↓
MPRNet (Supervised)	0.355 / 0.279 / 8.872	0.424 / 0.314 / 8.231	0.159 / 0.125 / 7.946
MPRNet + CSUD (Unsupervised)	0.228 / 0.213 / 9.874	0.271 / 0.241 / 9.452	0.151 / 0.124 / 7.532
NeRD-Rain-S (Supervised)	0.341 / 0.298 / 7.132	0.445 / 0.339 / 6.679	0.167 / 0.131 / 7.151
NeRD-Rain-S + CSUD (Unsupervised)	0.336 / 0.298 / 7.104	0.441 / 0.338 / 6.489	0.160 / 0.130 / 7.079
NAFNet (Supervised)	0.308 / 0.285 / 7.150	0.416 / 0.328 / 6.722	0.152 / 0.124 / 7.108
NAFNet + CSUD (Unsupervised)	0.258 / 0.257 / 8.103	0.345 / 0.295 / 7.622	0.141 / 0.120 / 7.369

Table 3. Ablation experiments on the numbers of GANs. All models in the table are trained on Rain100L, SPA-Data and RealRain1K-L are used to evaluate the model’s generalization capability. Bold fonts indicate the highest metrics.

Num of GANs	Rain100L PSNR ↑ / SSIM ↑	RealRain1K-L PSNR ↑ / SSIM ↑	SPA-data PSNR ↑ / SSIM ↑
1	31.87 / 0.919	28.11 / 0.906	33.13 / 0.932
2	32.92 / 0.948	29.08 / 0.923	33.67 / 0.936
4	33.28 / 0.954	29.21 / 0.928	33.57 / 0.939

the best LPIPS and DISTs with all the 3 baselines, and NeRD-Rain-S with CSUD maintains best results for all the 3 perceptual metrics on all the 3 datasets. This shows that the derained image obtained by our method can obtain higher perceptual quality, and further demonstrates the effectiveness and the generalization ability of our methods.

Effect of the additional 3 GAN constraints. The introduction of the additional 3 adversarial constraints aims to enhance the training stability and improve the network’s performance. To validate the necessity, we respectively train the model with 1, 2, and 4 adversarial constraints, with results shown in Tab. 3. It is obvious that when 4 GAN constraints are used, the deraining performance and generalization ability of the network are the best, demonstrating the effectiveness of the additional 3 GAN constraints. Note that, during inference, only the derainer is used and our framework does not introduce any additional inference overhead.

Separation training of our framework. In order to further explore whether our unsupervised framework can train the generator and the derainer separately, we first train the generator separately and then train the derainer with

Table 4. Ablation experiments on separation training of CSUD framework. All models in the table are trained on Rain100L. Bold fonts indicate the highest metrics.

Training Strategy	Rain100L PSNR ↑ / SSIM ↑	RealRain1K-L PSNR ↑ / SSIM ↑	SPA-data PSNR ↑ / SSIM ↑
Separate Training	31.06 / 0.947	29.06 / 0.928	32.39 / 0.936
Joint Training	33.28 / 0.954	29.21 / 0.928	33.57 / 0.939

the pseudo-paired rain-clean image generated by the trained generator. As shown in Tab. 4, although it can still achieve good performance under separate training, its deraining performance and generalization ability have significantly decreased compared to joint training. Many components in our framework rely on the collaborative interaction to make derainer and generator mutually enhance each other. If the generator and derainer are trained separately, the SRloss for derainer and additional GAN constraints cannot be added to training process, and the generator cannot continuously generate pseudo-paired data, which will cause reduced constraints and performance degradation.

7. Discussion and Limitations

Like other image deraining methods, our method also face the same problem that it may mistakenly remove some background textures similar to the rain streaks in real rainy images, this shortcoming needs to be further improved. Additionally, our method can be widely applied in many applications such as autonomous vehicles and video surveillance. Therefore, one should be cautious of questionable results and avoid infringement of privacy or negative impact on society.

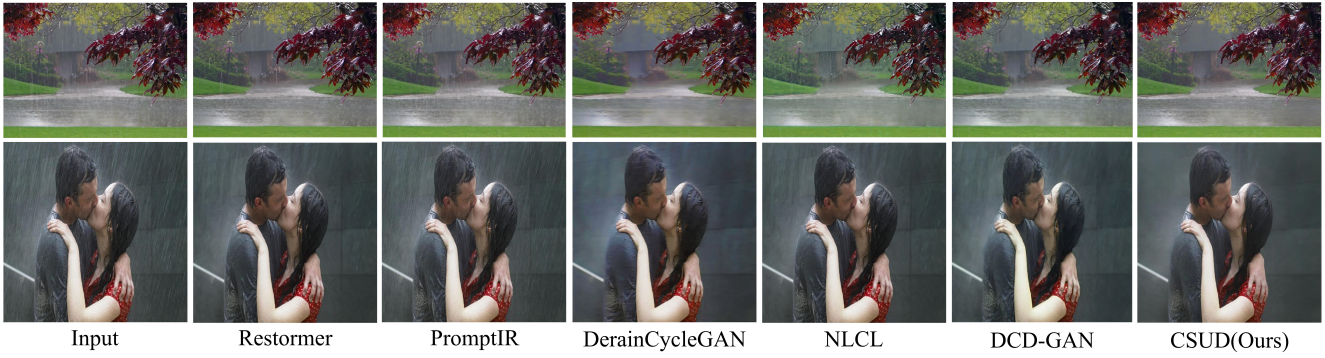


Figure 10. Qualitative generalization results on Internet-Data [39] dataset.

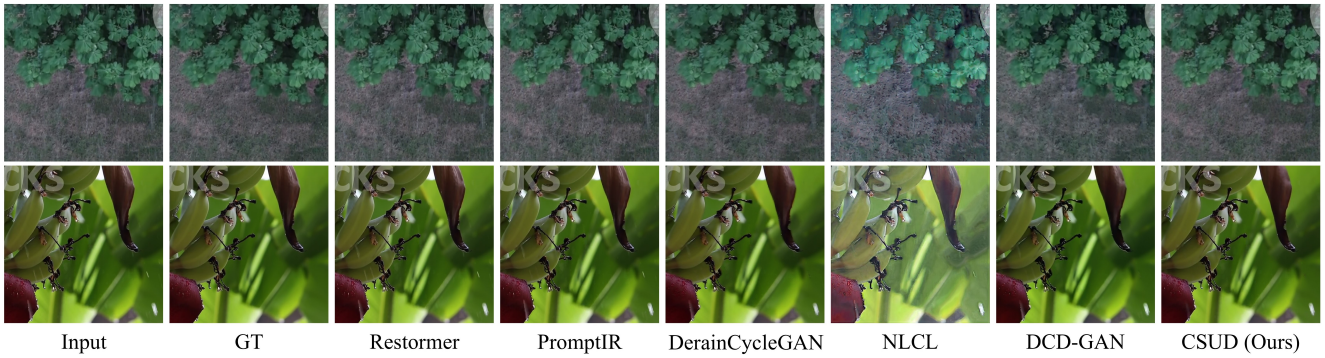


Figure 11. Qualitative generalization results on SPA-data [36] dataset.

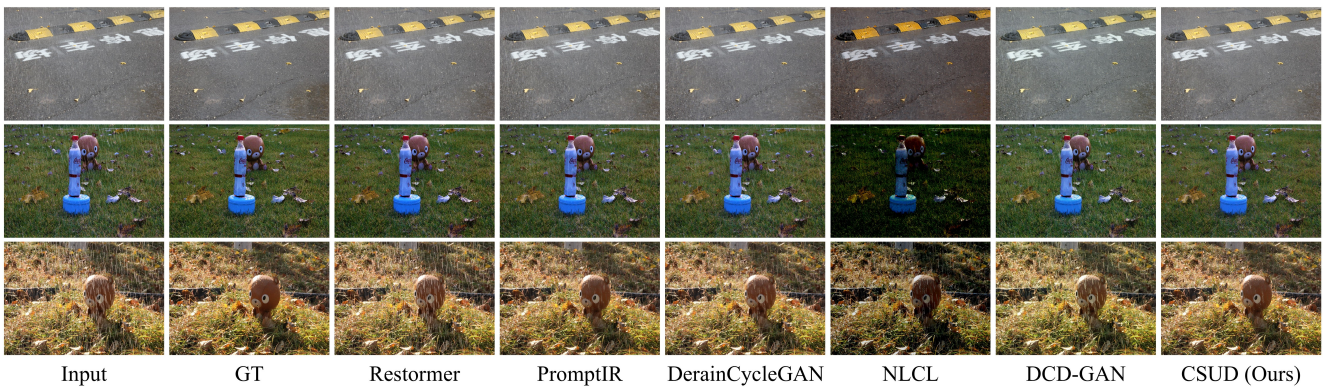


Figure 12. Qualitative generalization results on RainDS [30] dataset.